

Electronic Supplementary Information

Catalytic Metal-Induced Crystallization of Sol-Gel Metal Oxides for High-Efficiency Flexible Perovskite Solar Cells

Cheng-Hung Hou^a, Jing-Jong Shyue^{a,b}, Wei-Fang Su^a, Feng-Yu Tsai^{a*}

^a Department of Materials Science and Engineering, National Taiwan University, Taipei 106, Taiwan

^b Research Center for Applied Science, Academia Sinica, Taipei 115, Taiwan

*E-mail: ftsai@ntu.edu.tw

Experimental Section

Materials

All chemicals were commercially available and used as received, including nickel 2-ethylhexanoate (78% in ethylhexanoic acid, Sigma-Aldrich), titanium tetraisopropoxide (TTIP) (99.999%, Sigma-Aldrich), tin(IV) chloride pentahydrate (98 %, Sigma-Aldrich), PbI₂ (99.99%, Sigma-Aldrich), CH₃NH₂ (33 wt% in absolute ethanol, Sigma-Aldrich), HI (57 wt% in water, Sigma-Aldrich), PC₆₁BM (>99%, Solenne), polyethylenimine (PEI), (M_w:25000, branched, Sigma-Aldrich), and anhydrous solvents purchased from Sigma-Aldrich, including N,N-dimethylformamide (DMF), dimethylsulfoxide (DMSO), diethyl ether, chlorobenzene (CB), acetic acid, ethanol, and isopropanol.

Thin Film and Solar Cell Fabrication

To fabricate the Au nanoislands-embedded Ni_xO films, a 1 nm-thick Au film was first deposited on a substrate by thermal evaporation with a deposition rate of 2 Å per second under high vacuum (<3 × 10⁻⁴ Pa). The substrate was then transferred to a 150 °C hotplate for a 30 minutes annealing, where the Au film reflowed to become Au nanoislands. A Ni_xO films was spin-coated onto the Au nanoislands from 70 μl of 0.3 M nickel 2-ethylhexanoate solution in ethanol at 1700 rpm for 35 s in a glove box, followed by sintering at various temperatures in air for 5 h. The thickness of the sintered Ni_xO film was 50 nm as determined by cross-sectional TEM. The Au film-embedded Ni_xO films used for cross-sectional TEM, ToF-SIMS, and XPS analyses were fabricated with an identical process except that the thermally evaporated Au films were 50 nm thick and not annealed to induce reflow. The Ni and Pt films for c-MIC investigation in the sol-gel TiO_x and SnO_x systems were deposited by thermal evaporation and sputtering, respectively. The sol-gel TiO_x and SnO_x films were spin-coated from 70 μl of 1.0 M TTIP and 1.0M tin(IV) chloride pentahydrate

solution in a mixed-solvent (ethanol: acetic acid = 1:1 v/v), respectively, at 2000 rpm for 1 minute and then sintered at various temperatures in air.

The PSC devices were of the structure of glass/ITO/Ni_xO/MAPbI₃/PC₆₁BM/PEI/Ag and fabricated as follows. ITO-coated glass substrates ($10 \Omega \times \square^{-1}$, Ritek) cut into 1.0 × 1.5 cm rectangles were ultrasonically cleaned in turn in deionized water, acetone, and isopropanol. The Ni_xO HTL, either with embedded Au nanoisland or without it, was applied with the above-described procedure. The MAPbI₃ layer was spin-coated from 70 μl of 1.0M MAI/PbI₂ solution in DMF at 1,000 rpm for 5 s followed immediately with 4,000 rpm for 30 s. During the last 15 s of the latter spinning step, 350 μl of diethyl ether was gradually dispensed on the surface. The film was then dried on a hot plate at 60 °C for 2 minutes followed by another 2 min at 100 °C to crystallize the perovskite film. CH₃NH₃I (MAI) was synthesized from CH₃NH₂ and HI according to a previously reported method.¹ The PC₆₁BM layer was spin-coated from a CB solution of 20 mg ml⁻¹ concentration at 1200 rpm for 30 s. The PEI layer was spin-coated from an isopropanol solution of 0.1 wt % concentration at 3500 rpm for 30 s. The MAPbI₃, PC₆₁BM, and PEI layers were all spin-coated in a glove box. Finally, The Ag film with 100 nm of thickness nm was thermally evaporated through a mask under high vacuum ($<3 \times 10^{-4}$ Pa). The devices were encapsulated with a glass lid sealed at the circumference with a UV-curable glue (EPOS-G159, Orient Service Corp.) in a glove box. The glue was cured by illumination with a 100 W UV light (wavelength: 365 nm, UVP) for 5 minutes.

Characterizations

J-V characteristics of the PSC devices were measured with a Keithley 2400 source meter with a voltage step of 10 mV and a delay time of 50 ms under standard air mass 1.5 sunlight generated with a solar simulator (Newport 69920, integrated intensity: 100 mWcm⁻²). The devices were covered with a metal mask with an aperture area of 0.09 cm² to accurately define the effective area of the devices. The voltage scanning range was between -0.1 V and 1.2 V. For the continuous power measurement, a constant bias value which corresponded to the maximum PCE value during J-V scan was applied on the devices. A Newport 91150-KG5 reference cell was used for calibration before each measurement. IPCE spectra of the PSC devices were measured in DC mode using a lock-in amplifier with a current preamplifier under short-circuit condition. The monochromatic light was obtained from a 250 W quartz-halogen lamp (Osram) and a monochromator. GIXRD was conducted with a Rigafu TTRAX3 X-ray diffractometer (Rigaku, Japan) with Cu K α radiation. TEM and HRTEM images were obtained using a FEI Tecnail G2 F20 field-emission TEM system (FEI, USA). The cross-section TEM sample was prepared with a FEI Helios 600i focus ion beam system (FEI, USA). Simultaneous TGA/DSC data were collected by TA Q600 (TA instruments, USA). All samples were kept at 140 °C for 30 minutes before going to target temperature with a heating rate of +1 °C per minute. The Au nanoparticle (Au NP)-embedded samples for simultaneous TGA/DSC measurements were prepared by mixing the precursor with aqueous Au NP solution (100mg ml⁻¹). The UV-Vis spectra were measured with a Hitachi U-4100

spectrophotometer (Hitachi, Japan). XPS depth profiling was done with a PHI 5000 VersaProbe (ULVAC-PHI, Japan) using an Al K α X-ray source and a 3 kV Ar sputtering source (100 μ m, 25 W). ToF-SIMS depth profiling was obtained with a PHI TRIFT V nanoTOF system (ULVAC-PHI, Japan) using a pulsed (\sim 8000 Hz) bismuth liquid metal ion gun. Bi $_3^+$ ion beam with an acceleration bias of 30 kV and a beam current of 1.2 nA-DC was used to generate secondary ions. The secondary ions were accelerated to 3 kV by sample bias and transferred into a 2 m flight path with a 240 eV pass energy and an angular acceptance of \pm 20 $^\circ$. A 20 kV 5 nA of Gas cluster ion beam (GCIB) of Ar $_{2500}^+$ was used to etch through the depth of the sample to maximize the vertical spatial resolution during the dual-beam depth profiling.

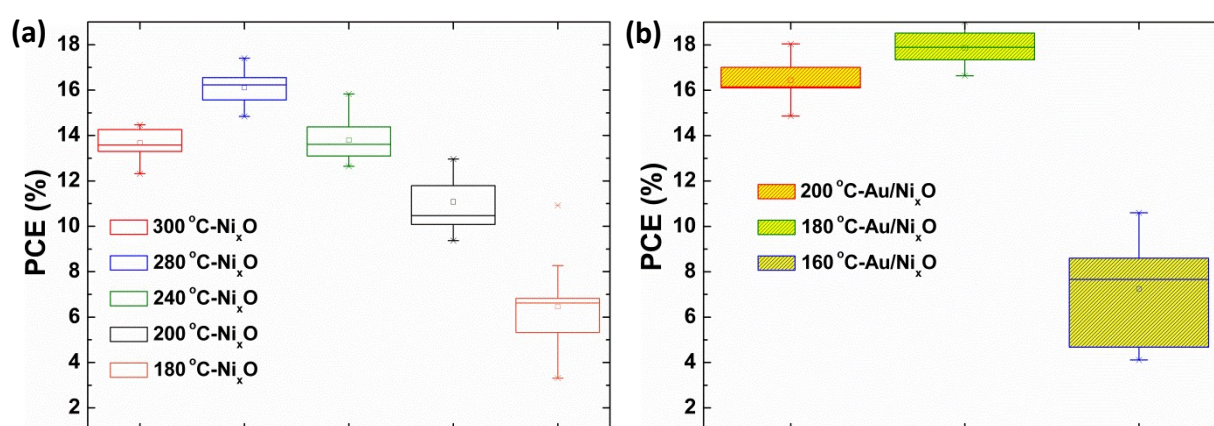


Figure S1: Box plots of the PCE values of all of the PSCs presented in Table 1 and Fig. 1: (a) PSCs with the regular Ni $_x$ O HTL; and (b) PSCs with the Au nanoislands-embedded Ni $_x$ O HTL.

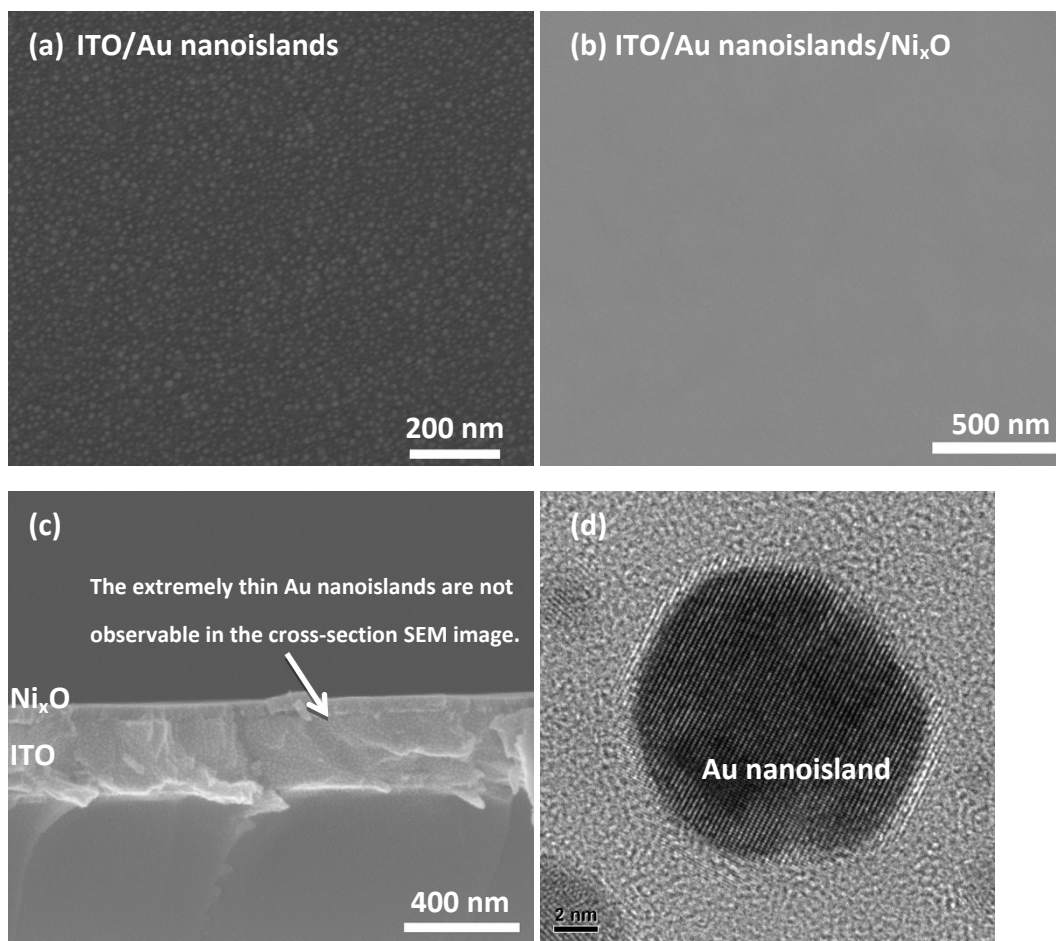


Figure S2: Top-view SEM images of (a) ITO/Au nanoislands and (b) ITO/Au nanoislands/Ni_xO; (c) cross-section SEM image of ITO/Au nanoislands/Ni_xO; (d) top-view HRTEM image of a single Au nanoisland (without Ni_xO).

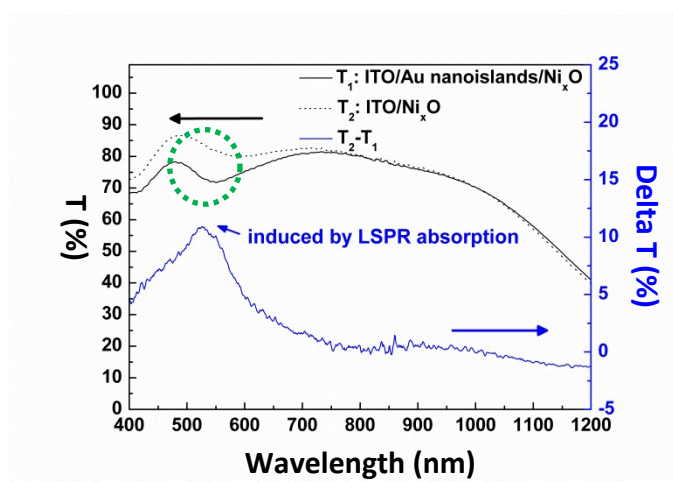


Figure S3: Optical transmittance of ITO/Au nanoislands/ Ni_xO (black line) and ITO/ Ni_xO (black dot).

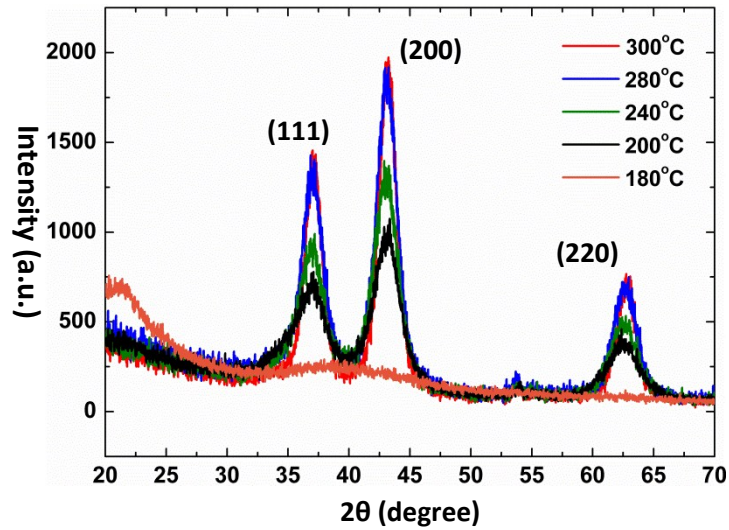


Figure S4: GIXRD patterns of Ni_xO film sintered at different temperatures.

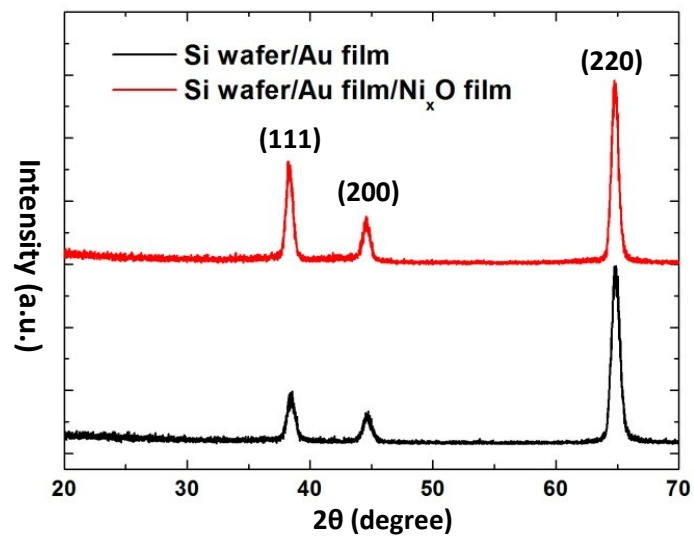


Figure S5: GIXRD patterns obtained from Si wafer/Au and 180 °C-sintered Si wafer/Au/sol-gel Ni_xO . Both sample show intense diffraction peaks at 35.7 °, 43.1 °, and 62.7 °, corresponding to the (111), (200), and (220) planes of either Au or NiO_x crystal.

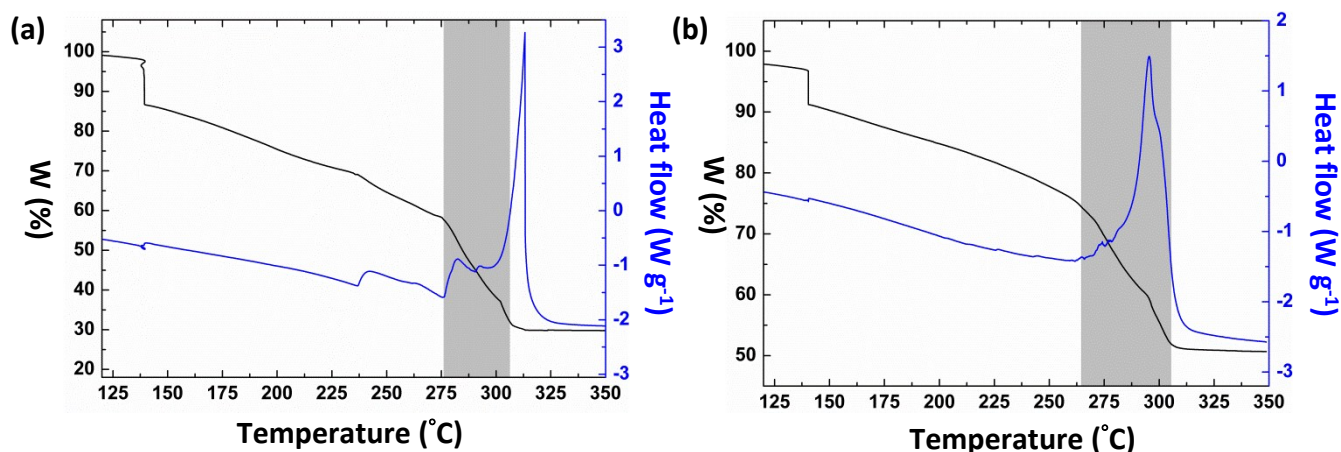


Figure S6: In-situ TGA/DSC analysis results during the sintering process of the NiO sol-gel precursor (a) without embedded Au; and (b) with embedded Au.

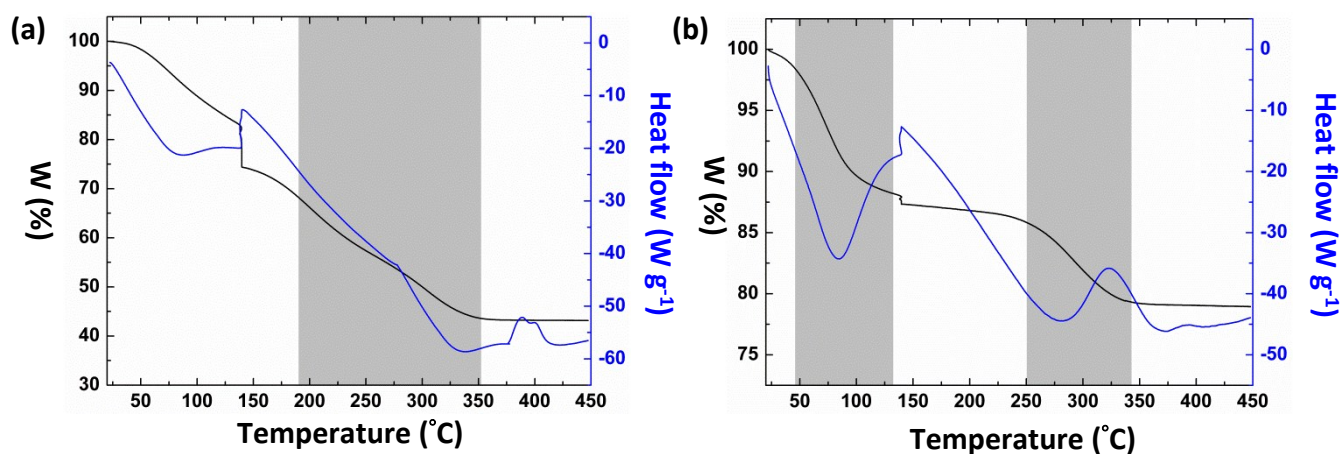


Figure S7: In-situ TGA/DSC analysis results during the sintering process of the TiO₂ sol-gel precursor (TTIP) (a) without embedded Au; and (b) with embedded Au.

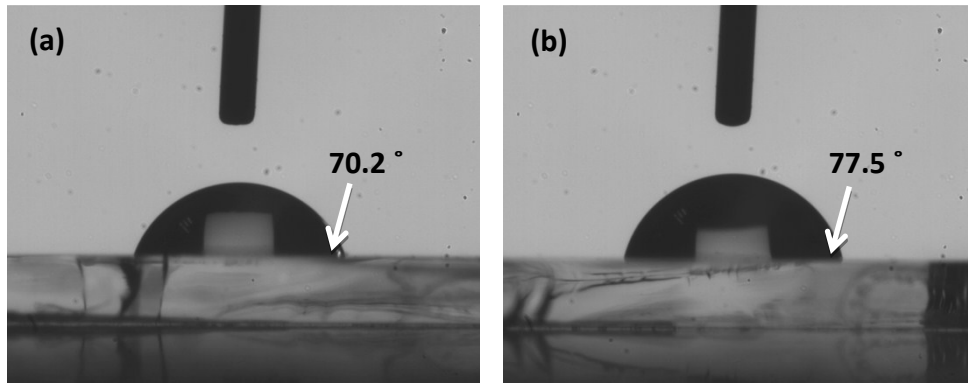


Figure S8: Water contact angles obtained from (a) 180 °C-annealed Au/NiO and (b) 280 °C -annealed NiO surface.

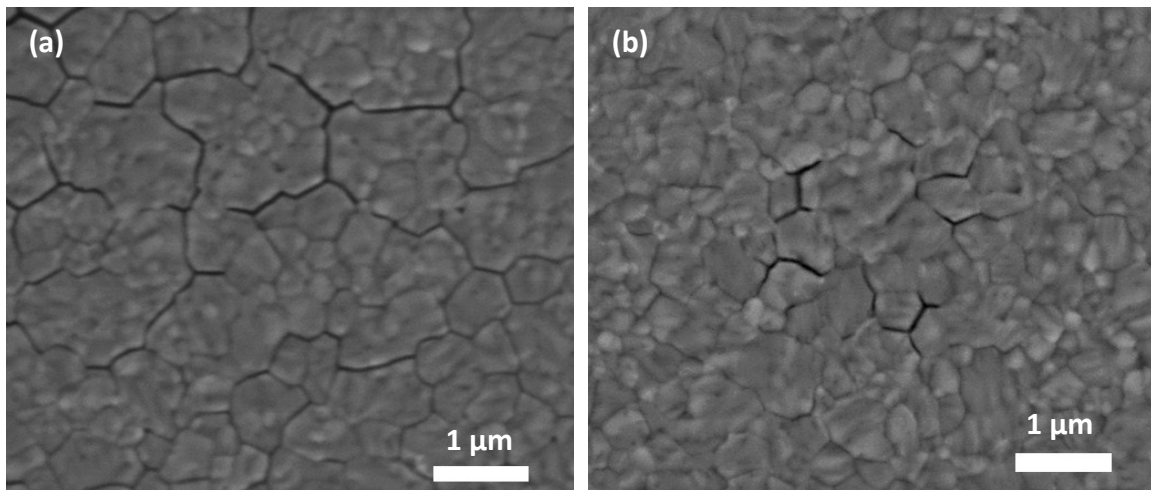


Figure S9: Top-view SEM images of perovskite layer deposited on (a) 180 °C-annealed Au/NiO and (b) 280 °C -annealed NiO surface.

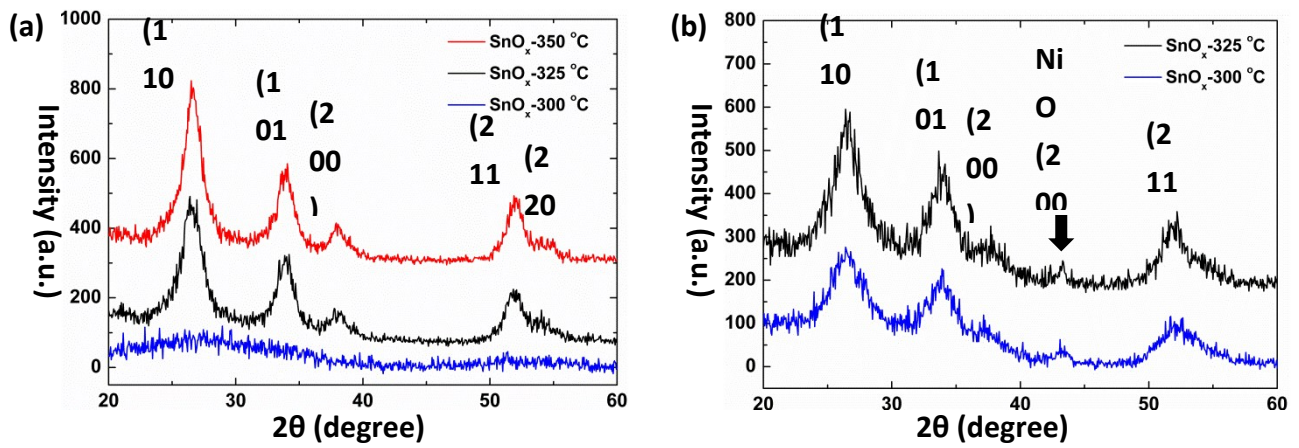


Figure S10: GIXRD patterns of sol-gel SnO_x films sintered at different temperatures: (a) without an embedded Ni film; and (b) with an embedded Ni film.

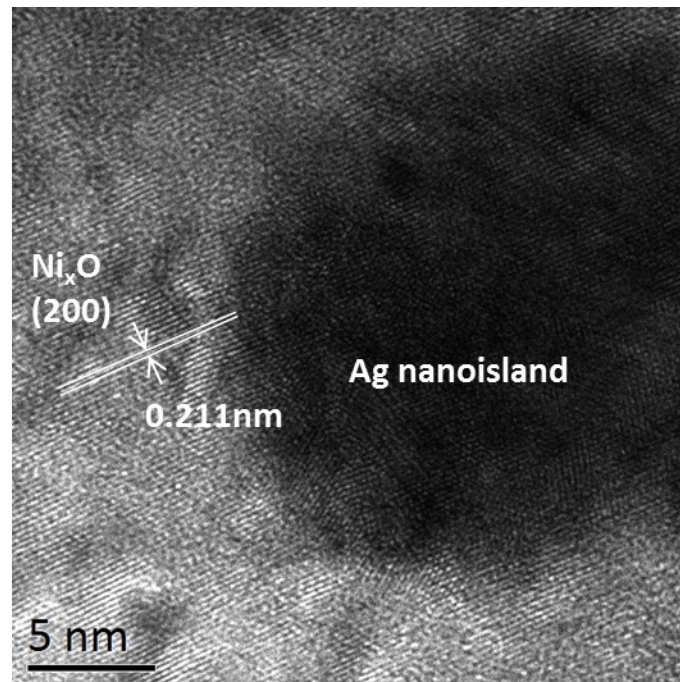


Figure S11: HRTEM image of 180 °C-sintered Ag nanoislands-embedded Ni_xO film. Lattice fringes originating from the (200) plane of the Ni_xO crystal (d-spacing = 0.211 nm) are as labeled.

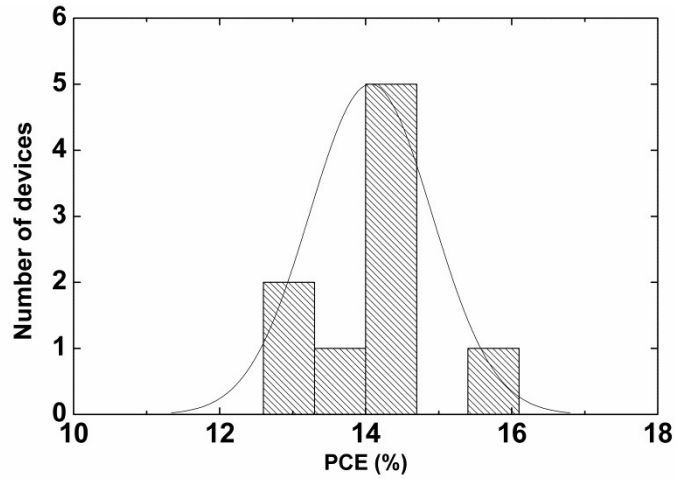


Figure S12: PCE Histogram of the 9 flexible PSCs which were used to calculate the average PCE of 14.0%.

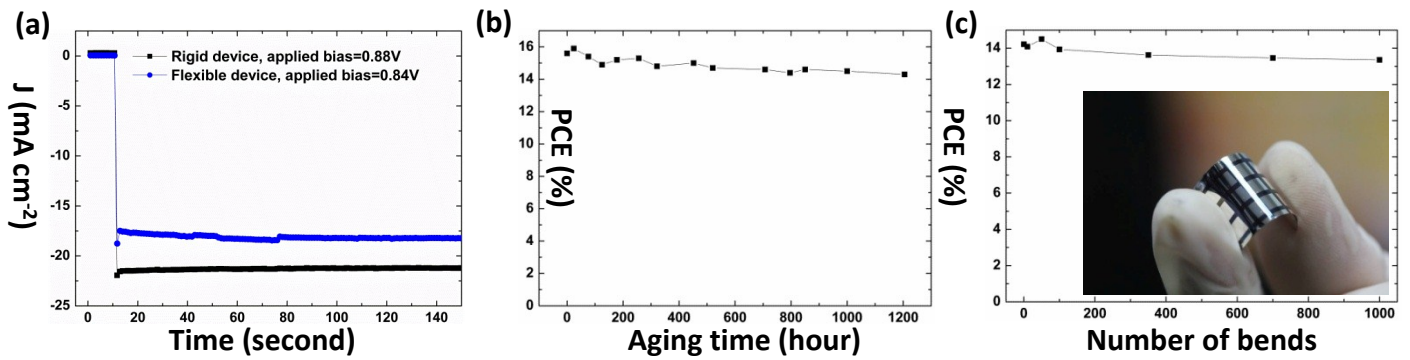


Figure S13 Additional device characteristics of the flexible PSCs shown in Fig. 8: (a) photocurrent density as a function of time under constant bias (results of a rigid device are also shown); (b) PCE as a function of time in an accelerated aging condition at 65 °C and 65% R.H.; (c) PCE as a function of the number of bends at 1.35 cm radius of curvature, with an inset showing a photo image of the bent device.

Reference

1. M. M. Lee, J. Teuscher, T. Miyasaka, T. N. Murakami and H. J. Snaith, *Science*, 2012, **338**, 643-647.